Reactive Template-Induced Core-Shell FeCo@C Microspheres as Multifunctional Electrocatalysts for Rechargeable Zinc-Air Batteries

Yanting Xu [1,†], Binling Chen [1,‡], Jun Nie, and Guiping Ma[*,†]

[†]State Key Laboratory of Chemical Resource Engineering, Key Laboratory of Carbon Fiber and Functional Polymers, Beijing University of Chemical Technology

[‡]College of Engineering, Mathematics and Physical Sciences, University of Exeter, Exeter, EX4 4QF, UK

Corresponding Author

[*]E-mail: magp@mail.buct.edu.cn

KEYWORDS: Core-shell, Fe-Co phosphide nanoparticles, Heteroatom-doped carbon, Electrocatalysts, Zn-air battery

Experimental Section

1. Synthesis

The mesoporous Fe_3O_4 microspheres were prepared via a solvothermal method according to a previous report.[S1] Typically, $FeCl_3$•$6H_2O$ (1.35 g) and NaAc (2.16 g) were dissolved in EG (33 ml) with magnetic stirring, followed by the addition of Na_3Cit (0.42 g) with continued vigorously stirring about 40 min. Then the homogeneous yellow solution was transferred into a Teflon-lined stainless-steel autoclave (50 ml capacity). The autoclave was heated to and kept at 200 ^oC for 8 h, and was cooled to room temperature naturally. The obtained precipitates were washed with absolute ethanol several times and then dried in a vacuum at 60 ^oC for 12 h.

Preparation of Fe_3O_4@PZS

The above synthesized Fe_3O_4 (0.06 g) were dispersed in 30 mL acetonitrile under ultrasound (50 Hz) for ten minutes to obtain a homogeneous suspension. Then 20 mL of acetonitrile containing 0.01 g of hexachlorocyclophosphazene and 0.05 g of 4,4'-sulfonyldiphenol was added into the above suspension. After ultrasound for ten minutes, trimethylamine (0.5 mL) was added to initialize the polymerization and the mixture was

ultrasounded continuously for another 3 h. When the reaction time was reached, the precipitates were collected and washed with ethanol for three times and dried in the oven under vacuum at 60 °C for 12 h. The obtained product was denoted as Fe_3O_4@PZS. The preparation of PZS was similar to the above process without the addition of Fe_3O_4.

Preparation of Fe_3O_4@PZS@ZIF-67

The Fe_3O_4@PZS@ZIF-67 was prepared by in situ growth method.[S2] The as-prepared Fe_3O_4@PZS (0.03 g) microspheres were dispersed into 10 mL of $Co(NO_3)_2$•$6H_2O$ (1 mM) methanol solution under ultrasound for 30 minutes and then the mixture was put in the oven under vacuum at 80 °C overnight to make the solvent evaporate absolutely. Then 10 mL of 2-MeIM (5 mM) methanol solution was added to the dried mixture and kept for 10 minutes at room temperature. Finally, the samples were separated by a permanent magnet, washed with absolute ethanol and dried under vacuum at 80 °C for 12 h. The sample was named Fe_3O_4@PZS@ZIF-67. The preparation of PZS@ZIF-67 and Fe_3O_4@ZIF-67 was similar to the above process.

Preparation of FeCo@C MS

The above obtained Fe_3O_4@PZS@ZIF-67 product was carbonized at 850°C with heating rate of 2 °C/min for 2 h in a tubular furnace under N_2 atmosphere. 10 mg of the obtained Fe_3O_4/Co-NPS was pre-leached in 10 mL 2 M HCl at 80°C for 12 h and washed thoroughly with deionized water and ethanol and dried under vacuum at room temperature for 12 h. The acid etched product was denoted as Fe/Co-NPS and carbonized at 850°C with heating rate of 2 °C/min for 2 h in a tubular furnace under N_2 atmosphere to get FeCo@C MS.

The preparation of Fe-NPS, Fe/Co-N, Co-NPS from Fe_3O_4@PZS, Fe_3O_4@ZIF-67, PZS@ZIF-67 was similar to the above process.

Preparation of Fe_3O_4-850

The prepared Fe_3O_4 was carbonized at 850°C with heating rate of 2 °C/min for 2 h in a tubular furnace under N_2 atmosphere. The obtained sample was denoted as Fe_3O_4-850.

Preparation of Fe_3O_4@NPS

The prepared Fe_3O_4@PZS was carbonized at 850°C with heating rate of 2 °C/min for 2 h in a tubular furnace under N_2 atmosphere. The obtained sample was denoted as Fe_3O_4@NPS.

2. Characterizations

Microscopic features of the above prepared samples were characterised by transmission electron microscope (TEM, Tecnai G^2 T20, FEI, USA) and high-resolution transmission electron microscope (HRTEM, JEM 3010, JEOL, Japan). Attenuated total reflectance-Fourier transform infrared (ATR-FTIR) spectra were collected using a spectrometer (Nicolet-is5 IR, Thermo Fisher Scientific, USA). The crystal structure was evaluated on a powder X-ray diffraction (XRD, D8 Advance, Bruker, Germany) system with Cu Kα radiation. The surface chemical composition of the microspheres was analyzed by X-ray photoelectric spectroscopy (XPS, ESCALAB 250, Thermo VG Scientific, USA). Nitrogen absorption/desorption isotherms were obtained on a analyzer (3H-2000PS1, Beishide Instrument Company) at 77 K and the corresponding surface areas were determined using the Brunauer-Emmett-Teller (BET) method. Energy dispersive X-ray spectroscopy (EDS, S-3200N, Hitachi, Japan) was performed to measure the composition of the samples at 1 KV. The internal structure and graphitic structure were also investigated by a Raman microscopy system (Invia Reflex, Renishaw, British). The Zn-air battery performance was performed by LAND CT2001A.

3. Electroncatalytic evaluation

The electrochemical tests were performed in a standard three-electrode system controlled by a CHI 760E electrochemistry workstation. Catalyst powders coated on glassy carbon (GC, 5 mm diameter) and RRDE (5 mm diameter) were used as working electrode, platinum slice as counter electrode and saturated calomel electrode as reference electrode. All the potentials

of HER and OER in this work were *iR*-corrected, and all the potentials (vs SCE) were converted to the RHE scale using the Nernst equation ($E_{RHE} = E_{SCE} + 0.244 + 0.0591$ pH). The GC and RRDE electrodes were polished with alumina slurries and subsequently washed with ultrapure water and ethanol.

Preparation of working electrode

All prepared catalysts (5 mg) were ultrasonically dispersed in the mixture of ethanol (1 mL) and 5% Nafion (100 μL) to form catalyst ink, respectively. And a 10 μL (for GC) or 5 μL (for RRDE) of the catalyst ink was dropped onto the polished electrode and dried at room temperature. The 20 wt% Pt/C catalyst was also coated on the GC or RRDE electrode in the same way as a benchmark for the electrochemical activity.

ORR and OER activity tests

ORR activity measurements were carried out at room temperature both in 0.10 M KOH solution and 0.5 M H_2SO_4 solution. OER activity tests were carried out in 0.10 M KOH solution. Before test, a O_2 flow was used for the electrolyte for 30 min to give a saturation state. Cyclic voltammetry for ORR was carried out in O_2-saturated 0.1 M KOH from 0.21 V to 0.11 V and O_2-saturated 0.5 M H_2SO_4 from 0 V to 1.2 V at a scan rate of 50 mV s^{-1}. Cyclic voltammetry for OER was carried out in O_2-saturated 0.1 M KOH from 1.0 V to 2.1 V. Linear sweep voltammograms (LSV) measurements for ORR were performed at different rotating speeds from 400 to 2500 rpm in O_2-saturated 0.1 M KOH from 0 V to 1.2 V and O_2-saturated 0.5 M H_2SO_4 from 0 V to 1.2 V at a sweep rate of 10 mV s^{-1}. LSV measurements for OER were performed in O_2-saturated 0.1 M KOH from from 1.0 V to 2.1 V with a rotation speed of 1600 rpm. The RRDE was used in 0.10 M KOH solution and the GC was used in 0.5 M H_2SO_4 solution as the substrate for the working electrode.

The number of electrons transferred onto the catalyst was calculated according to the Koutecky-Levich equation:

$$\frac{1}{j} = \frac{1}{j_D} + \frac{1}{j_K} = \frac{1}{(B\omega^{1/2})} + \frac{1}{j_K}$$

$$B = 0.2nFC_0D_0^{2/3}v^{-1/6}$$

where j (mA cm^{-2}) is the measured current density, which is related to the diffusion-limiting current (j_d) and the kinetic current (j_k), F is the Faraday constant (96485 C mol^{-1}), D_O is the diffusion coefficient of oxygen in 0.1 M KOH (1.9×10^{-5} cm^2 s^{-1}), v is the kinematic viscosity of water (0.01 cm^2 s^{-1}), C_O is the bulk concentration of oxygen in oxygen-saturated 0.1 M KOH (1.2×10^{-6} mol cm^{-3}), ω is the rotation rate, and n is the electron transfer number for the ORR. A linear plot of j_{lim}^{-1} versus $\omega^{-1/2}$ has a slope of $1/(0.2nFC_0D_0^{2/3}v^{-1/6})$.

The four-electron selectivity of catalysts was evaluated based on the H_2O_2 yield, calculated from the following equation:

$$H_2O_2(\%) = 200 \times \frac{I_R/N}{(I_R/N) + I_D}$$

The electron transfer number can be calculated from the following equation:

$$n = 4 \times \frac{I_D}{(I_R/N) + I_D}$$

Here, I_D and I_R are the disk and ring currents, respectively, and $N = 0.37$ is the ring collection efficiency. Chronoamperometric measurements were performed at a static cathodic potential (0.71 V) and an electrode rotation speed of 1600 rpm in O_2-saturated 0.10 M KOH solution to investigate stability and possible poisoning effect of the catalysts.

HER activity tests

To evaluate HER activity, the electrochemical tests were performed in 0.5 M H_2SO_4 solution which were purged with high purity nitrogen gas for at least 30 mins before measurement. Catalyst powders coated on GC were used as working electrode and the

electrode was constantly rotating at 1600 rpm to get rid of the bubbles during measurement. Linear sweep voltammetry was carried out at the scan rate of 5 mV s^{-1}. Electrochemical impedance spectroscopy was measured at the overpotential of 0.2 V in the frequency range of 10^{5}-10^{-2} Hz with the amplitude potential of 5 mV. The stability of prepared catalyst was evaluated by chronopotentiometry at 10 mA cm^{-2}.

4. Zn-air Battery Performance

The rechargeable Zn-air battery performance was measured using a liquid Zn-air battery with catalysts on carbon paper as the cathode, a polished Zn plate (0.3 mm of thickness) as anode, and 6 M KOH solution as the electrolyte for both primary and rechargeable Zn-air batteries.[S3,4] Typically, 100 μL catalyst ink was dropped onto carbon paper and dried naturally to form a uniform catalyst layer, resulting a mass loading of 1.2 mg cm^{-2}. For comparison, the performance of the Zn-air battery containing 20 wt% Pt/C and RuO_2 (20 wt% Pt/C + RuO_2) with the mass ratio of 1:1 was also tested under similar conditions. The battery test was performed in room environment on LAND CT2001A.

Supporting Figures

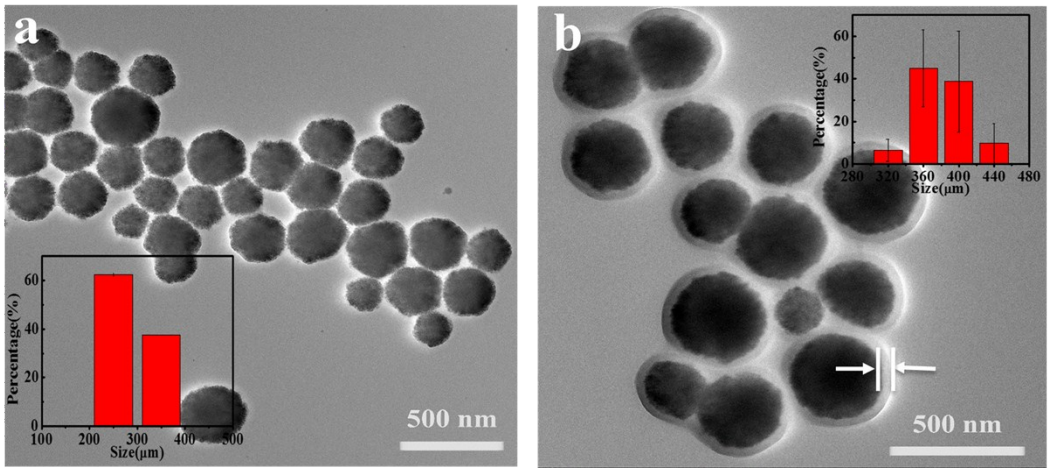

Figure S1. TEM images of (a) Fe_3O_4 and (b) Fe_3O_4@PZS.

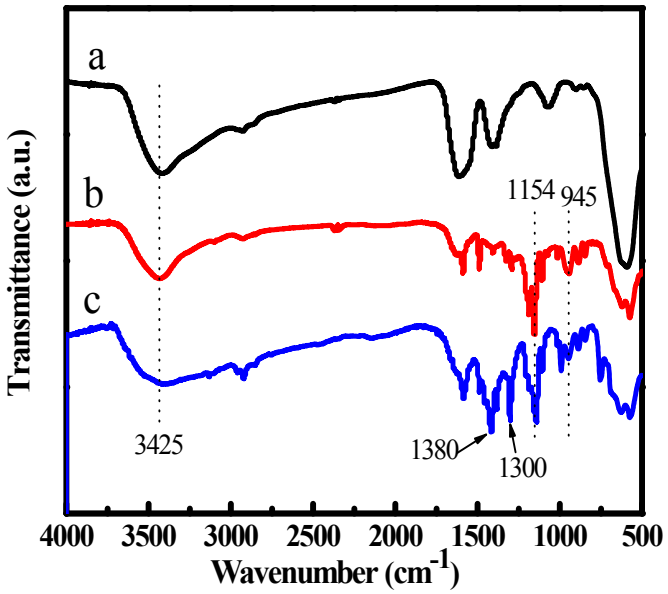

Figure S2. FT-IR spectra of (a) Fe_3O_4, (b) Fe_3O_4@PZS and (c) Fe_3O_4@PZS@ZIF-67.

To prove the formation of core-shell and core-double shell structure, the FT-IR detection was conducted. As can be seen in Figure S2a, the absorption peak at around 580 cm^{-1} was the characteristic peak for Fe-O. The peak at 3425 cm^{-1} was the stretching vibration of -OH on the surface of Fe_3O_4. New peaks centred at 945 and 1154 cm^{-1} appeared in Figure S2b, which can be assigned to the new produced P-O-(Ph) and S=O in BPS respectively. The peaks at 525 and 607 cm^{-1} were the characteristic peaks for P-Cl in HCCP. Therefore, it can be concluded that the PZS shell was coated on the surface of Fe_3O_4 core. As shown in Figure S2c, the new strong peaks at 1300 and 1380 cm^{-1} can be attributed to the C-N and -CH_3 in 2-Methylimidazole, which proved that ZIF-67 was grown on the surface of Fe_3O_4@PZS.

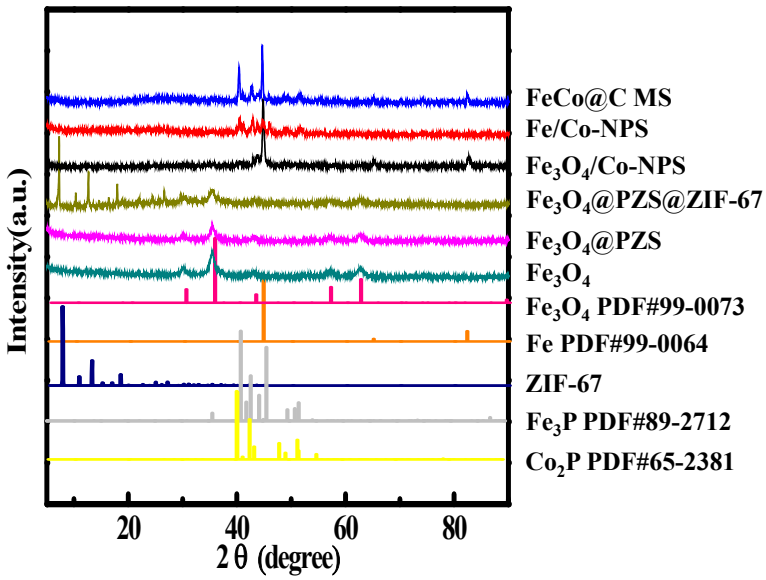

Figure S3. XRD patterns of samples obtained.

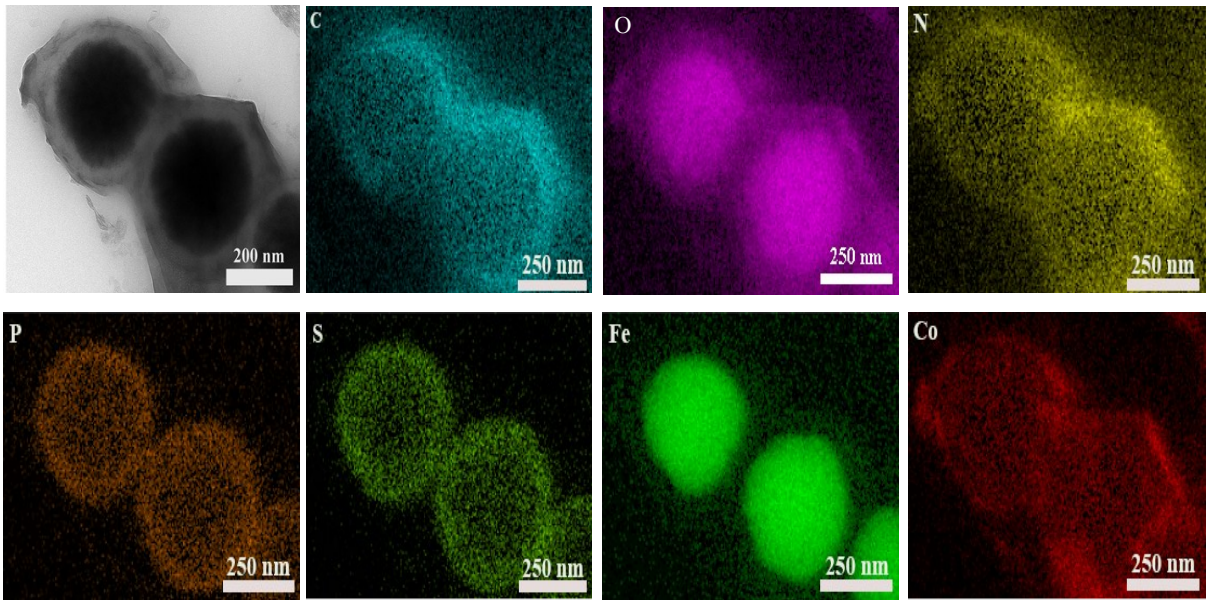

Figure S4. Compositional EDS mapping of Fe_3O_4@PZS@ZIF-67 using scanning transmission electron microscopy.

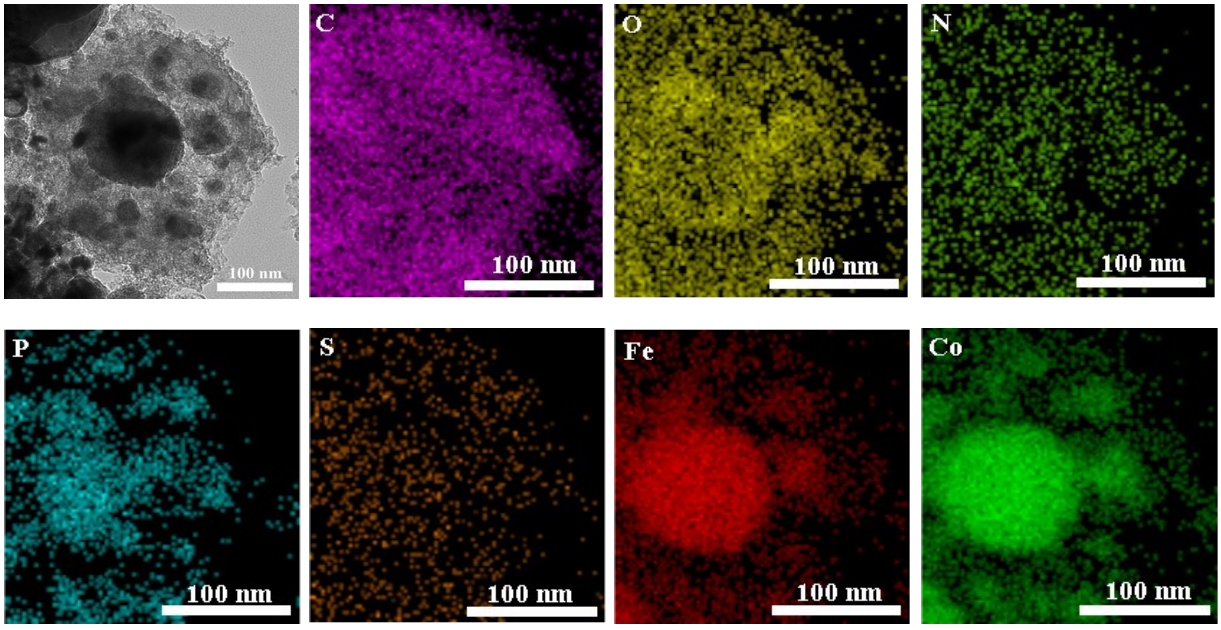

Figure S5. Compositional EDS mapping of Fe_3O_4/Co-NPS using scanning transmission electron microscopy.

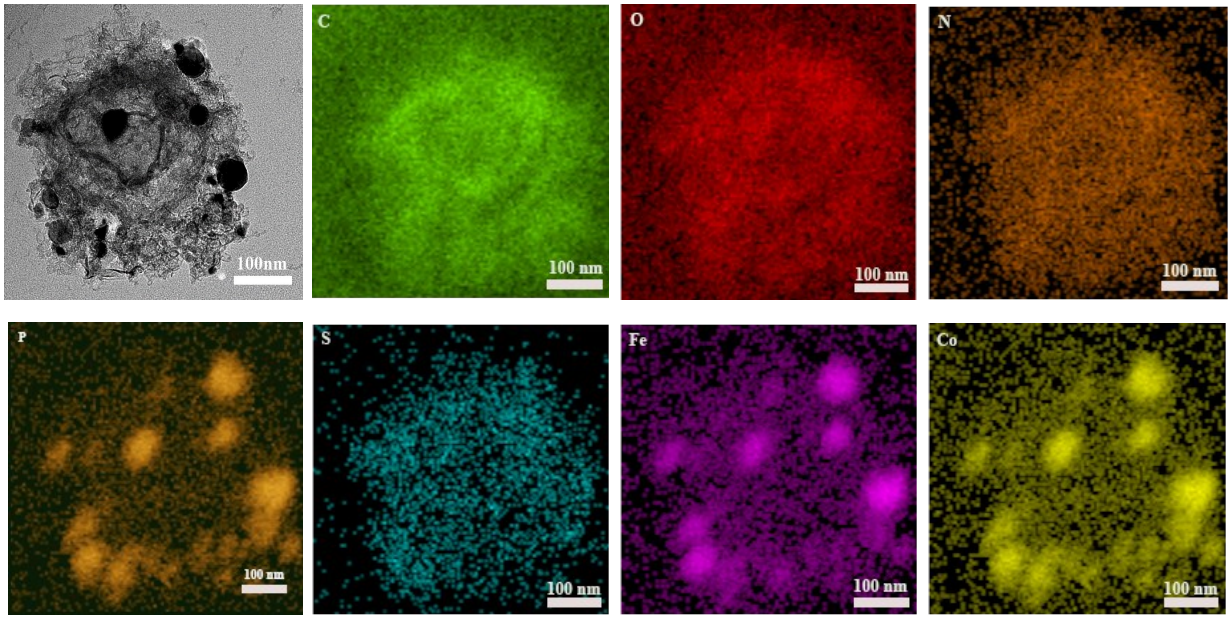

Figure S6. Compositional EDS mapping of Fe/Co-NPS using scanning transmission electron microscopy.

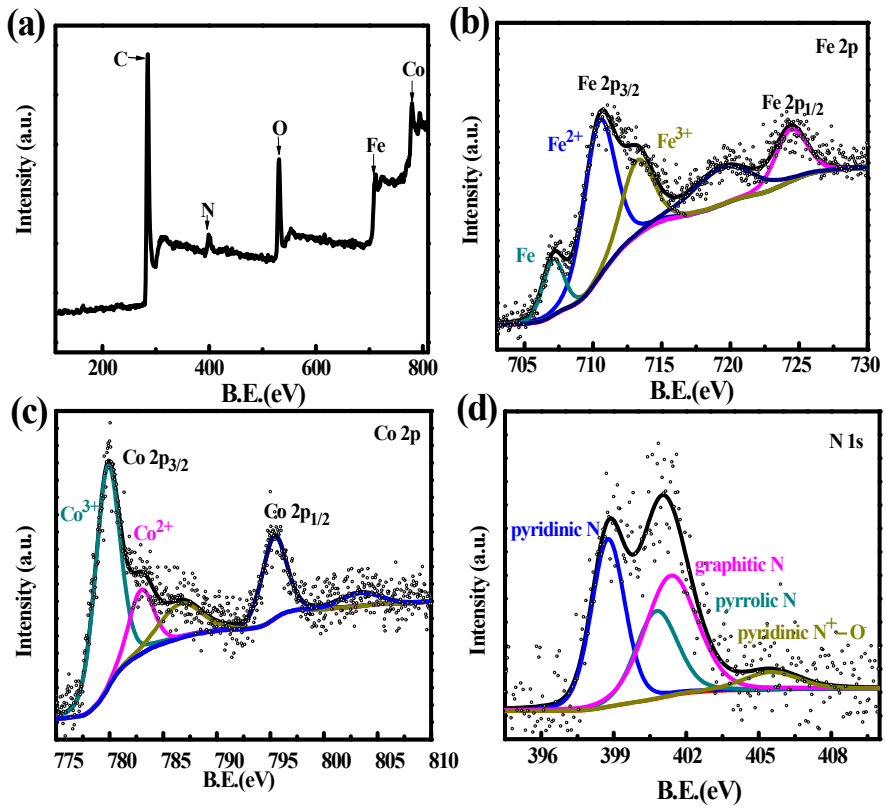

Figure S7. (a) Full spectrum and high-resolution XPS spectra of (b) Fe 2p, (c) Co 2p, and (d) N 1s of Fe_3O_4/Co-NPS.

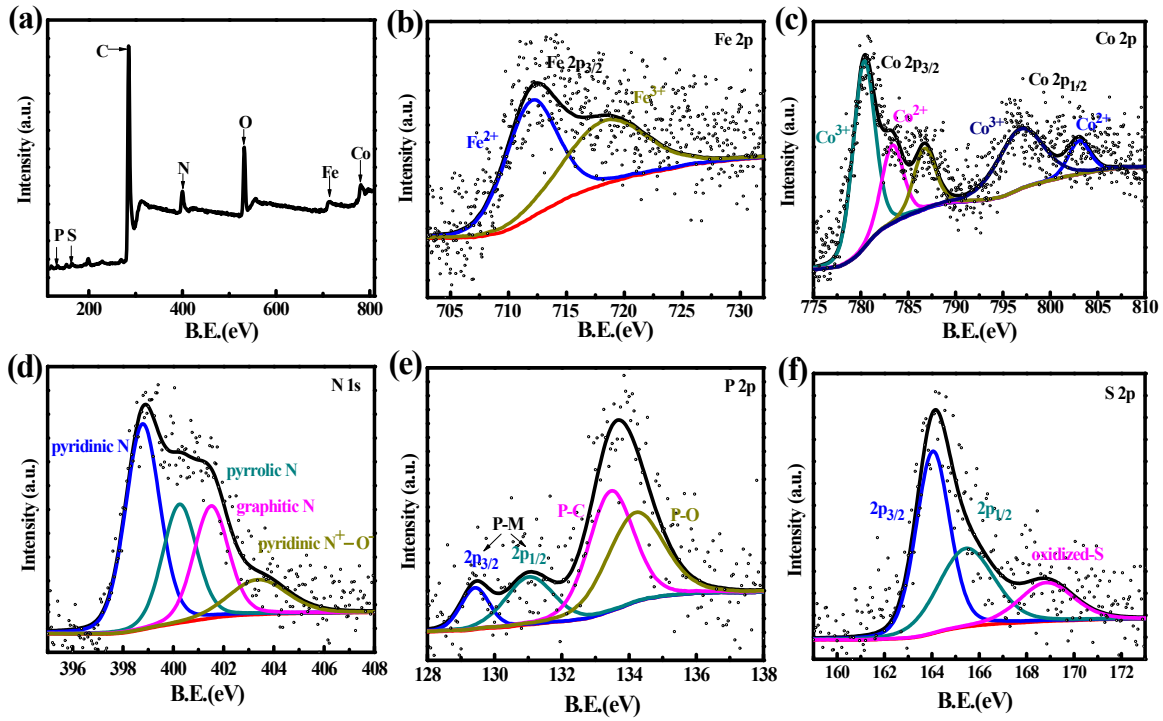

Figure S8. (a) Full spectrum and high-resolution XPS spectra of (b) Fe 2p, (c) Co 2p, (d) N 1s, (e) P 2p, and (f) S 2p of Fe/Co-NPS.

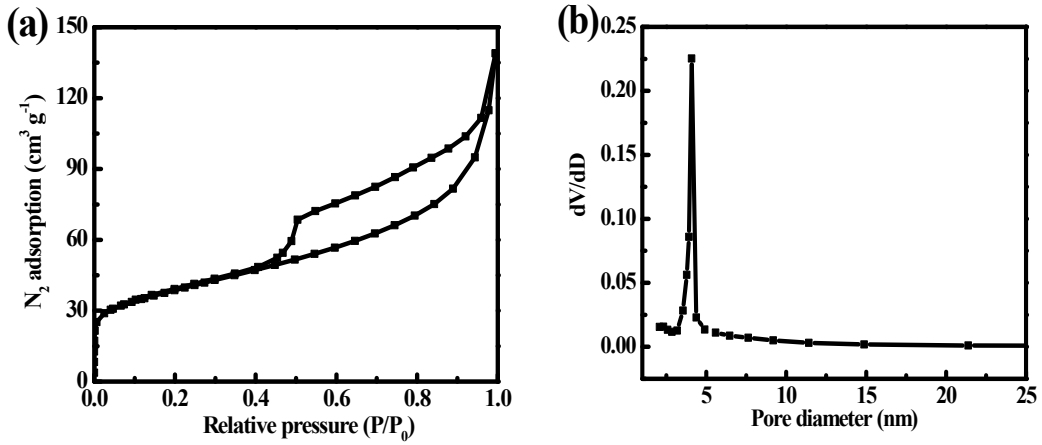

Figure S9. (a) Nitrogen adsorption-desorption isotherms of Fe_3O_4/Co-NPS, and (b) its corresponding pore-size distribution.

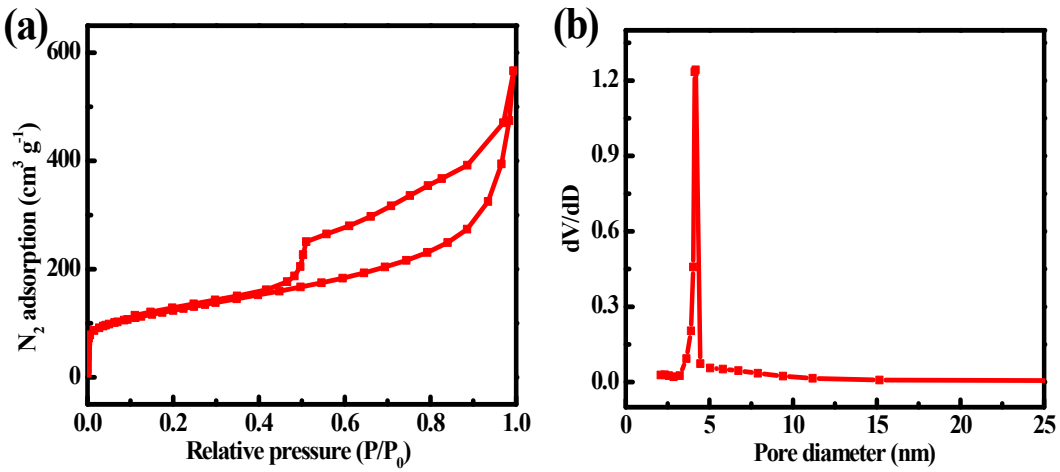

Figure S10. (a) Nitrogen adsorption-desorption isotherms of Fe/Co-NPS, and (b) its corresponding pore-size distribution.

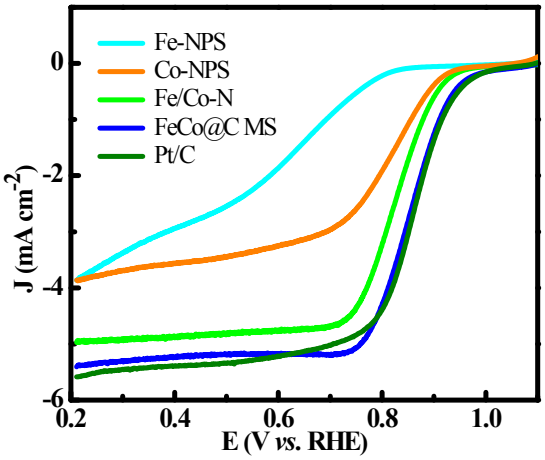

Figure S11. LSV plots of Fe-NPS, Fe/Co-N, Co-NPS, FeCo@C MS and Pt/C at a scan rate of 10 mV s^{-1} with a rotation speed of 1600 rpm in O_2-saturated 0.1 M KOH.

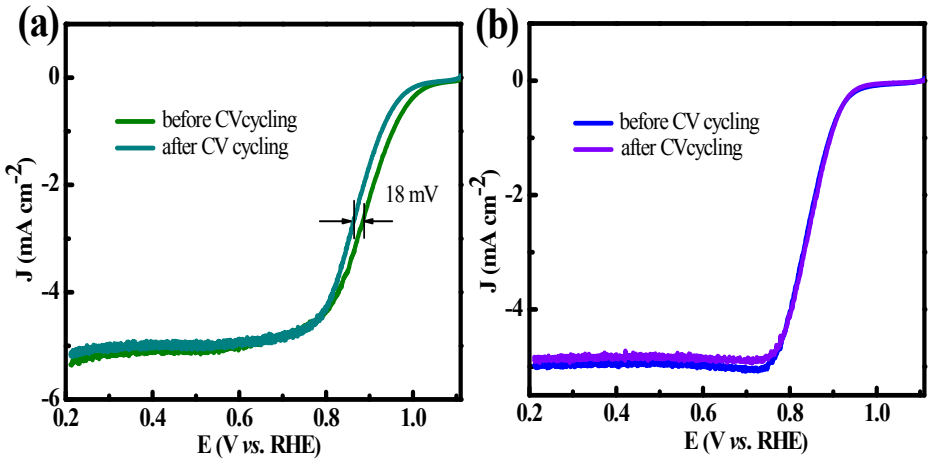

Figure S12. ORR LSV curves of (a) Pt/C and (b) FeCo@C MS before and after CV cycling for 1000 cycles at 50 mV s^{-1} within the potential range from 0.21 to 1. 1 1V.

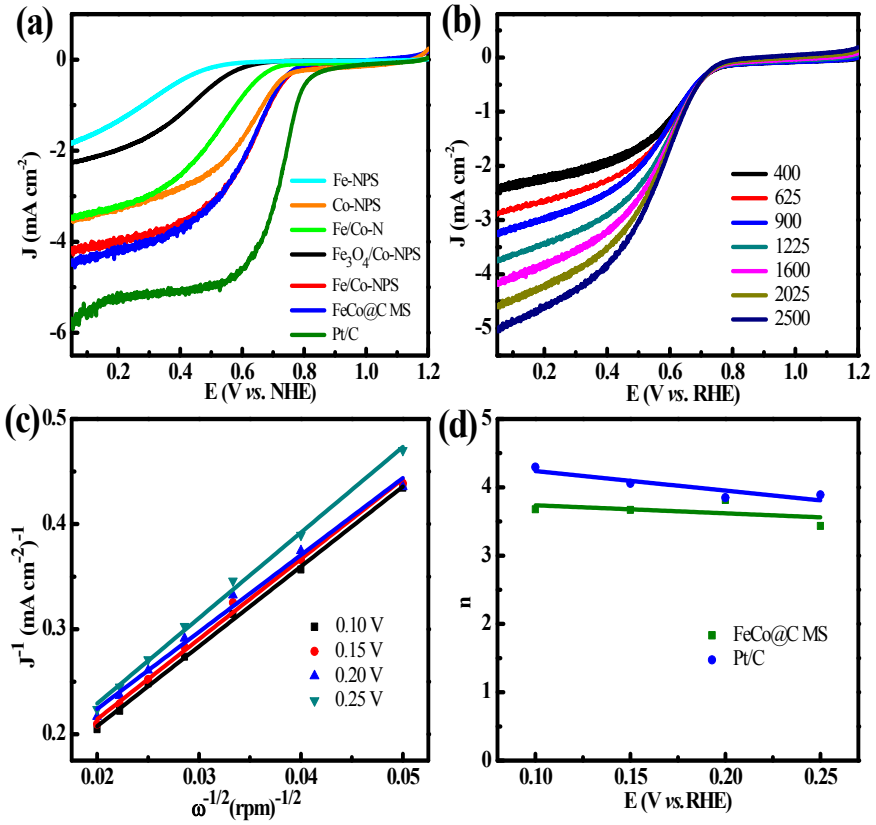

Figure S13. Electrochemical evaluation of Fe_3O_4/Co-NPS, Fe/Co-NPS, FeCo@C MS and commercial Pt/C catalysts in O_2-saturated 0.5 M H_2SO_4. (a) RRDE polarization plots of Fe_3O_4/Co-NPS, Fe/Co-NPS, FeCo@C MS and commercial Pt/C catalysts at a scan rate of 10 mV s^{-1} with a rotation speed of 1600 rpm. (b) Voltammograms of FeCo@C MS at various speeds at a scan rate of 10 mV s^{-1}. (c) Corresponding Koutecky-Levich plots at different potentials. (d) Electron transfer number of FeCo@C MS and commercial Pt/C.

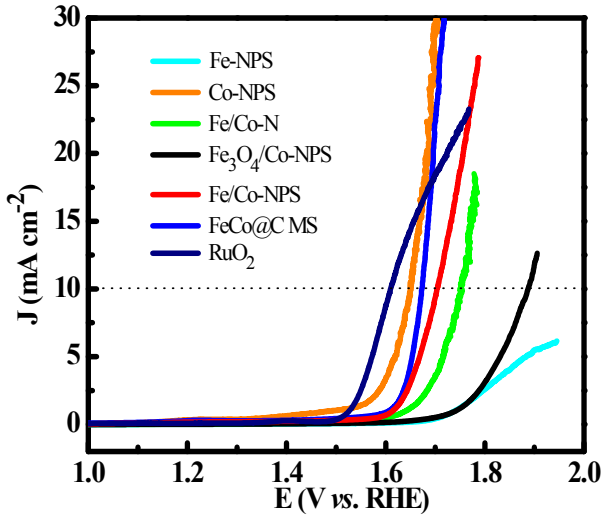

Figure S14. Polarization plots for OER of Fe_3O_4/Co-NPS, Fe/Co-NPS and FeCo@C MS catalysts at a scan rate of 10 mV s^{-1} with a rotation speed of 1600 rpm in O_2-saturated 0.1 M KOH.

Table S1. Textural properties of Fe_3O_4/Co-NPS, Fe/Co-NPS and FeCo@C MS.

Catalyst	BET specific surface area (m^2/g)	Pore volume (cm^3/g)	Pore diameter (nm)
Fe_3O_4/Co-NPS	133.4	0.2	4.1
Fe/Co-NPS	428.9	0.9	4.2
FeCo@C MS	465.8	1.2	4.1

Table S2. Summary of ORR performance of recently reported core-shell catalysts.

Catalyst	E_0 (V *vs.*RHE)	$E_{1/2}$ (V *vs.*RHE)	Condition	Reference
Pt/C	1.02	0.86	0.1 M KOH	This work
FeCo@C MS	1.04	0.85	0.1 M KOH	This work
CoOx@NC	0.91	0.72	0.1 M KOH	S5
CoOx@C	0.75	0.68	0.1 M KOH	S5
CoS NWs@NSC-2	0.93	0.84	0.1 M KOH	S6
CNF@Zn/CoNC	0.91	0.82	0.1 M KOH	S7
CNF@CoNC	0.89	0.81	0.1 M KOH	S7
CNF@ZnNC	0.87	0.78	0.1 M KOH	S7
$F_{0.2}N_{0.2}M_{0.2}$-900	0.97	0.87	0.1 M KOH	S8
Co@CoOx/NCNTs	0.94	0.80	0.1 M KOH	S9
Fe@C-NG/NCNTs	0.93	0.84	0.1 M KOH	S10
CoZn-NC-700	0.98	0.84	0.1 M KOH	S3
Fe-Phen-N-800	0.99	0.86	0.1 M KOH	S11

Table S3. Summary of OER performance of recently reported catalysts which have core-shell structures.

Catalyst	E_0 (V *vs.*RHE)	Overpotential at 10 mA cm^{-2} (V *vs.*RHE)	Condition	Reference
RuO_2	1.48	0.38	0.1 M KOH	This work
FeCo@C MS	1.53	0.44	0.1 M KOH	This work
CoOx@NC	1.41	0.35	0.1 M KOH	S5
CoOx@C	1.53	0.39	0.1 M KOH	S5
CNF@Zn/CoNC	1.52	0.47	0.1 M KOH	S7
CNF@CoNC	1.53	0.48	0.1 M KOH	S7
CNF@ZnNC	1.42	0.55	0.1 M KOH	S7
$F_{0.2}N_{0.2}M_{0.2}$-900	1.21	0.42	0.1 M KOH	S8
Fe@C-NG/NCNTs	1.42	0.45	1 M KOH	S10
CoZn-NC-700	1.52	0.39	0.1 M KOH	S3
Ni/Fe_3O_4@ONC	1.46	0.30	0.1 M KOH	S12

Table S4. Summary of HER performance of recently reported catalysts which have core-shell structures.

Catalyst	Overpotential at 10 mA cm^{-2} (V *vs.*RHE)	Tafel slope ($mV\ dec^{-1}$)	Condition	Reference
Pt/C	0.03	29	0.5 M H_2SO_4	This work
FeCo@C MS	0.22	65	0.5 M H_2SO_4	This work
Fe_xP@NPC	0.23	81	0.5 M H_2SO_4	S13
C_3N_4@NG	0.24	52	0.5 M H_2SO_4	S14
FeCo@NCNTs-NH	0.30	74	0.5 M H_2SO_4	S15
G-coated Cu NWs	0.25	67	0.5 M H_2SO_4	S16
MoS_2/MoO_3/FTO	0.31	55	0.5 M H_2SO_4	S17
MoO_3/Ni_3S_2	0.30	57	0.5 M H_2SO_4	S18
Ni-Sn@C	0.36	35	0.5 M H_2SO_4	S19
MoS_2@MoO_2	0.24	76	0.5 M H_2SO_4	S20
Fe/P/C0.5-800	0.26	53.6	0.5 M H_2SO_4	S21

References

(S1) Meng, F.; Wang, Z.; Zhong, H.; Wang, J.; Yan, J.; Zhang, X. Reactive multifunctional template-induced preparation of Fe-N-doped mesoporous carbon microspheres towards highly efficient electrocatalysts for oxygen reduction. *Adv. Mater.*, **2016**, *28*, 7948-7955.

(S2) Niu, Q.; Guo, J.; Chen, B.; Nie , J.; Guo, X.; Ma, G. Bimetal-organic frameworks/polymer core-shell nanofibers derived heteroatom-doped carbon materials as electrocatalysts for oxygen reduction reaction. *Carbon*, **2017**, *114*, 250-260.

(S3) Chen, B.; He, X.; Yin, F.; Wang, H.; Liu, D.; Shi, R.; Chen, J.; Yin, H. MO-Co@N doped Carbon (M = Zn or Co): Vital roles of inactive Zn and highly efficient activity toward oxygen reduction/evolution reactions for rechargeable Zn-air battery. *Adv. Funct. Mater.* **2017**, *27*, 1700795.

(S4) Liu, J.; Jiang, L.; Tang, Q.; Wang, E.; Qi, L.; Wang, S.; Sun, G. Amide-functionalized carbon supports for cobalt oxide toward oxygen reduction reaction in Zn-air battery. *Appl. Catal. B-Environ.*, **2014**, *148*, 212-220.

(S5) Hao, Y.; Xu, Y.; Han, N.; Liu, J.; Sun, X. Boosting the bifunctional electrocatalytic oxygen activities of coox nanoarrays with a porous N-doped carbon coating and their application in Zn-air batteries. *J. Mater. Chem. A*, **2017**, *5*, 17804-17810.

(S6) Han, C.; Li, Q.; Wang, D.; Lu, Q.; Xing, Z.; Yang, X. Cobalt sulfide nanowires core encapsulated by a N,S-co-doped graphitic carbon shell for efficient oxygen reduction reaction. *Small*, **2018**, *14*, 1703642.

(S7) Zhao, Y.; Lai Q.; Zhu J .; Zhong J.; Tang Z.; Luo Y.; Liang Y. Controllable construction of core-shell polymer@zeolitic Imidazolate frameworks fiber derived heteroatom doped carbon nanofber network for effcient oxygenelectrocatalysis, *Small,* **2018**, *14*, e1704207.

(S8) Yang, W.; Zhang, Y.; Liu, X.; Chen, L.; Jia, J. In situ formed Fe-N doped metal organic framework@carbon nanotubes/graphene hybrids for a rechargeable Zn-air battery. *Chem. Commun.,* **2017**, *53*, 12934-12937.

(S9) Lin, C.; Shinde, S. S.; Jiang, Z.; Song, X.; Sun, Y.; Guo, L. In situ directional formation of Co@CoO_x-embedded in 1D carbon nanotubes as an efficient oxygen electrocatalyst for ultra-high rate Zn-air batteries. *J. Mater. Chem. A*, 2017, *5*, 13994-14002

(S10) Lei, Y.; Wang, Q.; Chen, Z.; Wu, N.; Wang, Y.; Wang, B. Fe/Fe_3C@C nanoparticles encapsulated in N-doped graphene-cnts framework as an efficient bifunctional oxygen electrocatalyst for robust rechargeable Zn-air batteries. *J. Mater. Chem. A,* **2017**, *6*(2).

(S11) Yang, Z.; Zhao, Z.; Liang, K.; Zhou, X.; Shen, C. C.; Liu, Y. N. Synthesis of nanoporous structured iron carbide/Fe-N-carbon composites for efficient oxygen reduction reaction in Zn-air batteries. *J. Mater. Chem. A*, **2016**, *4*, 19037-19044.

(S12) Liu, G.; Yao, R.; Zhao, Y.; Wang, M.; Li, N.; Li, Y. Encapsulation of Ni/Fe_3O_4 heterostructures inside onion-like N-doped carbon nanorods enables synergistic electrocatalysis for water oxidation. *Nanoscale,* **2018**, *10*(8), 3997.

(S13) Cheng, Y.; Guo, J.; Huang, Y.; Liao, Z.; Xiang, Z. Ultrastable hydrogen evolution electrocatalyst derived from phosphide postmodified metal-organic frameworks. *Nano Energy,* **2017***, 35*, 115-120.

(S14)Zheng, Y.; Jiao, Y.; Zhu, Y.; Li, L. H.; Han, Y.; Chen, Y. Hydrogen evolution by a metal-free electrocatalyst. *Nat. Commun.*, **2014**, *5,* 3783.

(S15) Deng, J.; Ren, P.; Deng, D.; Yu, L.; Yang, F.; Bao, X. Highly active and durable non-precious-metal catalysts encapsulated in carbon nanotubes for hydrogen evolution reaction. *Energy & Environ. Sci.*, **2014**, *7*, 1919-1923.

(S16) Arumugam, M.; Ling, L.; Wang, C. Y.; Chen, C. W.; Chen, Y. Z.; Medina, H. Graphene-coated copper nanowire networks as a highly stable transparent electrode in harsh

environments toward efficiently electrocatalytic hydrogen evolution reaction. J. *Mater. Chem. A*, **2017**, *5*, 13320-13328.

(S17) Chen, Z.; Cummins, D.; Reinecke, B. N.; Clark, E.; Sunkara, M. K.; Jaramillo, T. F. Core-shell MoO_3-MoS_2 nanowires for hydrogen evolution: a functional design for electrocatalytic materials. *Nano Letters,* **2011**, *11*(10), 4168-75.

(S18) Lu, W.; Song, Y.; Dou, M.; Ji, J.; Wang, F. Ni_3S_2@ MoO_3 core/shell arrays on Ni foam modified with ultrathin cds layer as a superior electrocatalyst for hydrogen evolution reaction. *Chem. Comm.,* **2017***, 54*(6).

(S19) Lang, L.; Shi, Y.; Wang, J.; Wang, F. B.; Xia, X. H. Hollow core-shell structured Ni-SN@C nanoparticles: a novel electrocatalyst for the hydrogen evolution reaction. *ACS Appl. Mater. Inter.,* **2015**, *7(17)*, 9098-9102.

(S20) Yang, L.; Zhou, W.; Hou, D.; Zhou, K.; Li, G.; Tang, Z. Porous metallic moo - supported mos nanosheets for enhanced electrocatalytic activity in the hydrogen evolution reaction. *Nanoscale,* **2015***, 7(12)*, 5203-5208.

(S21) Li, M.; Liu, T.; Bo, X.; Zhou, M.; Guo, L.; Guo, S. Hybrid carbon nanowire networks with Fe-P bond active site for efficient oxygen/hydrogen-based electrocatalysis. *Nano Energy,* **2017**, *33*, 221-228.